

Electronic Supplementary Information

Synthesis of New Stable and Metastable Thiocyanato Coordination Polymers by Thermal Decomposition and by Solution Reactions.

Susanne Wöhlert, Jan Boeckmann, Inke Jess and Christian Näther

Figure S1	Difference plot of $[\text{Cd}(\text{NCS})_2(\text{pyridine})_2]_n$ (2-Cd/III).	3
Figure S2	Calculated X-ray powder pattern (XRPD) of $\text{Cd}(\text{NCS})_2$ (A) and experimental X-ray powder pattern of the residue formed in the second TG step in the thermal decomposition reaction of 1-Cd (B) as well as of 2-Cd/III calculated from Rietveld refinement (C).	3
Figure S3	Crystal structure of 2-Cd/II .	4
Figure S4	Crystal structure of 2-Cd/III .	4
Figure S5	Crystal structure of 2-Cd/IV .	5
Figure S6	Experimental X-ray powder pattern (XRPD) of a mixture single crystals of 2-Cd/II and 2-Cd/IV (A) and X-ray powder pattern of 2-Cd/II (B) as well as 2-Cd/IV (C) calculated from single crystal data.	6
Figure S7	DSC curve for $\text{Cd}(\text{NCS})_2(\text{pyridine})_4$ (1-Cd).	6
Figure S8	DSC heating and cooling cycles for $[\text{Cd}(\text{NCS})_2(\text{pyridine})_2]_n$ (2-Cd/II).	7
Figure S9	DSC heating and cooling cycles for $[\text{Cd}(\text{NCS})_2(\text{pyridine})_2]_n$ (2-Cd/III).	7
Figure S10	DSC heating and cooling cycles for $[\text{Cd}(\text{NCS})_2(\text{pyridine})_2]_n$ (2-Cd/IV).	8
Figure S11	X-ray powder pattern of the intermediates obtained at different temperatures in the DSC measurement of compound 2-Cd/II and calculated X-ray powder pattern of $[\text{Cd}(\text{NCS})_2(\text{pyridine})_2]_n$ (2-Cd/II).	8
Figure S12	X-ray powder pattern of the intermediates obtained at different temperatures in the DSC measurements of compound 2-Cd/III and X-ray powder pattern of $[\text{Cd}(\text{NCS})_2(\text{pyridine})_2]_n$ (2-Cd/III) calculated from Rietveld refinement and of $\text{Cd}(\text{NCS})_2$ calculated from single-crystal data.	9
Figure S13	X-ray powder pattern of the intermediate obtained at 77 °C from the DSC measurement of compound 2-Cd/IV as well as the X-ray powder pattern calculated for $[\text{Cd}(\text{NCS})_2(\text{pyridine})_2]_n$ (2-Cd/IV) from single-crystal data.	9

Figure S14	IR spectrum of $\text{Cd}(\text{NCS})_2(\text{pyridine})_4$ (1-Cd).	10
Figure S15	IR spectrum of compound $[\text{Cd}(\text{NCS})_2(\text{pyridine})_2]_n$ (2-Cd/II).	10
Figure S16	IR spectrum of compound $[\text{Cd}(\text{NCS})_2(\text{pyridine})_2]_n$ (2-Cd/III).	11
Figure S17	IR spectrum of compound $[\text{Cd}(\text{NCS})_2(\text{pyridine})_2]_n$ (2-Cd/IV).	11
Figure S18	IR spectrum of compound $[\text{Cd}(\text{NCS})_2(\text{pyridine})]_n$ (3-Cd).	12

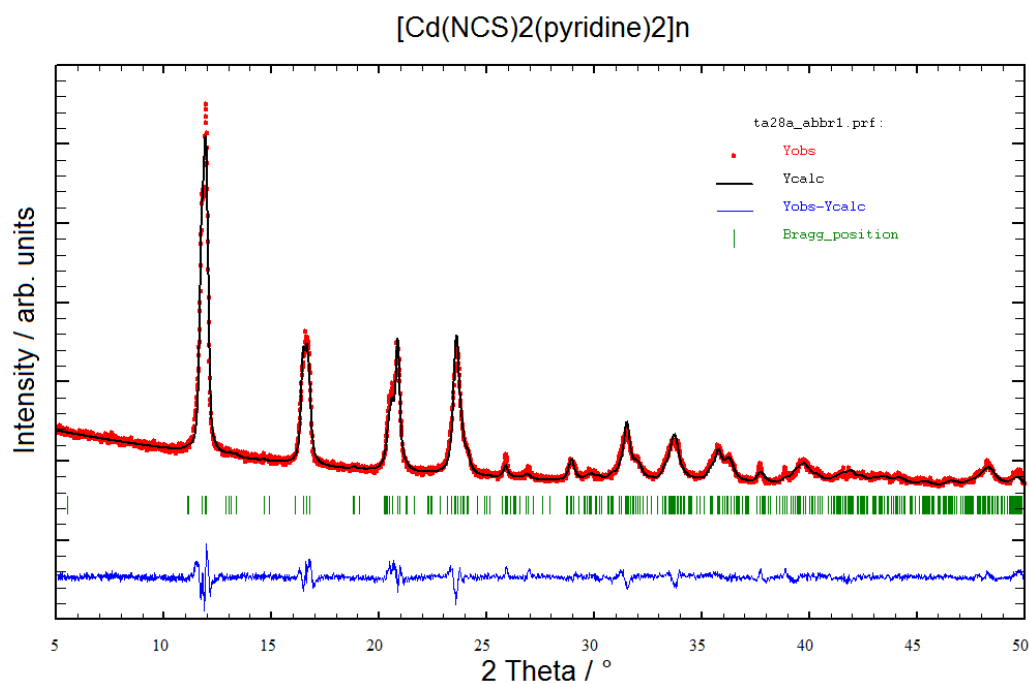


Figure S1. Difference plot of [Cd(NCS)₂(pyridine)₂]_n (**2-Cd/III**).

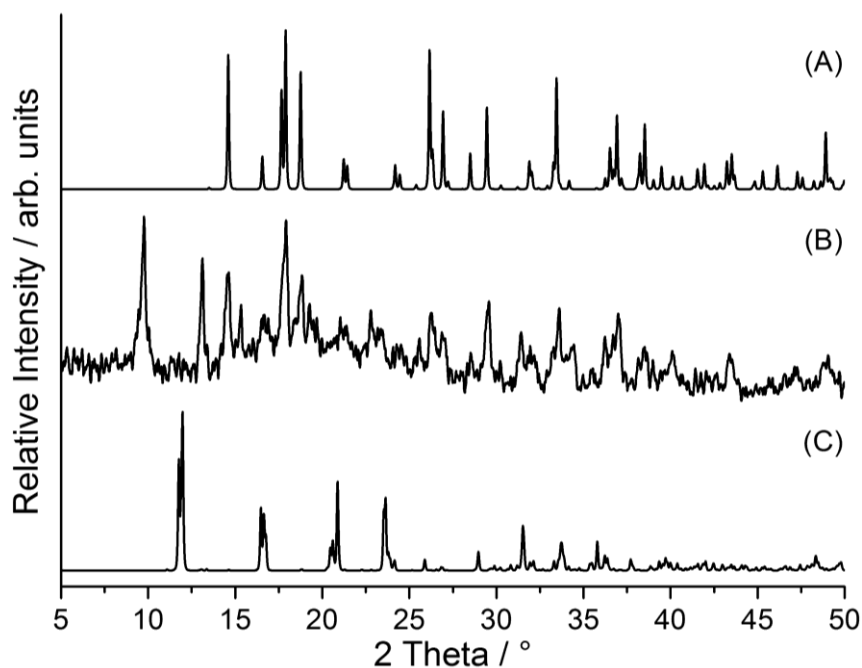


Figure S2. Calculated X-ray powder pattern (XRPD) of Cd(NCS)₂ (A) and experimental X-ray powder pattern of the residue formed in the second TG step in the thermal decomposition reaction of **1-Cd** (B) as well as of **2-Cd/III** calculated from Rietveld refinement (C).

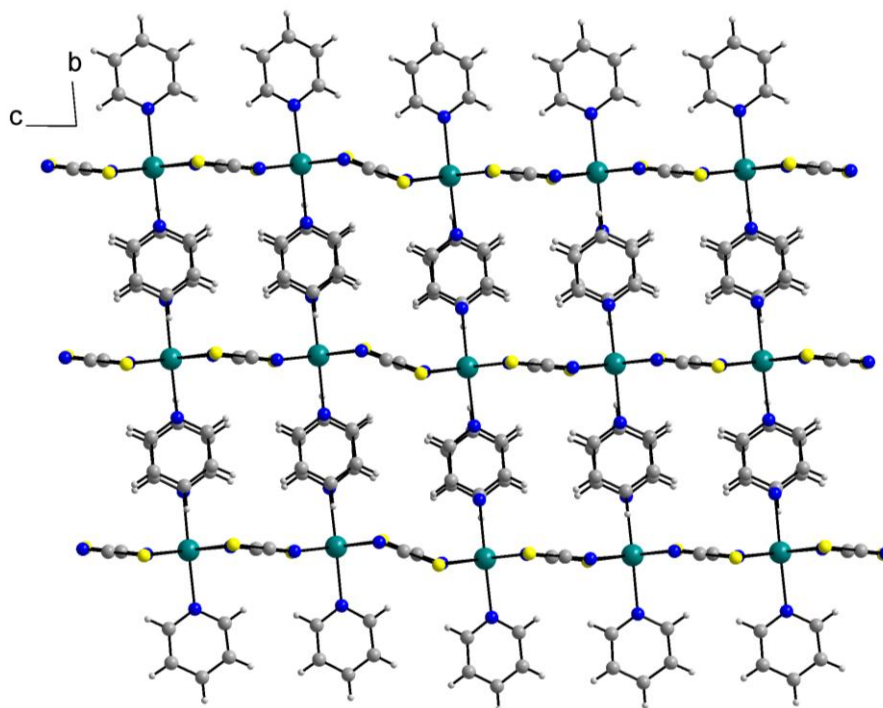


Figure S3. Crystal structure of **2-Cd/II** with view along the crystallographic *a*-axis (green = cadmium, blue = nitrogen, yellow = sulfur, grey = carbon, white = hydrogen).

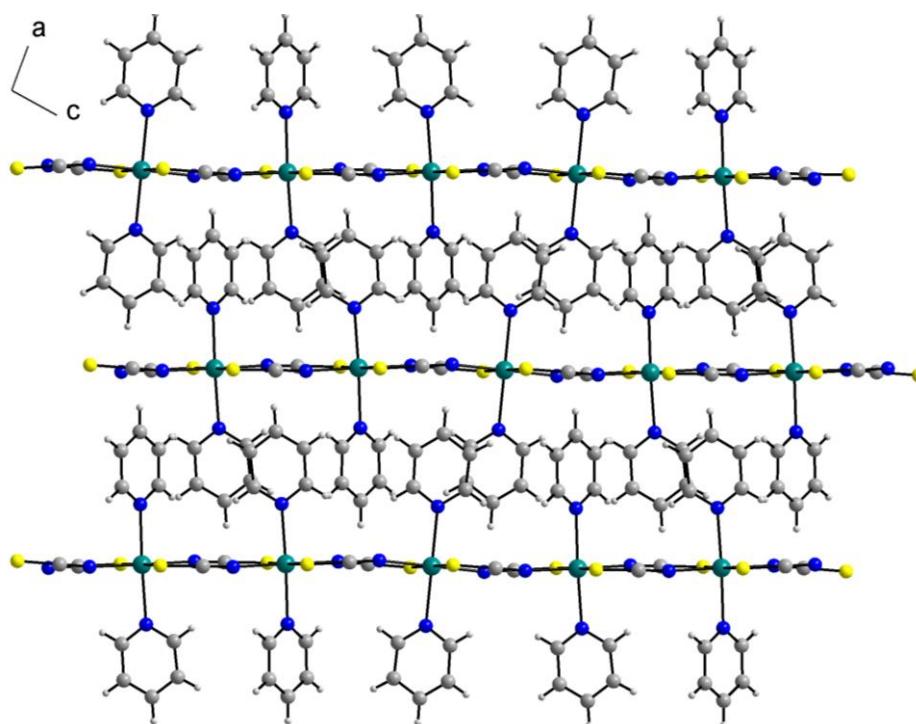


Figure S4. Crystal structure of **2-Cd/III** with view along the crystallographic *b*-axis (green = cadmium, blue = nitrogen, yellow = sulfur, grey = carbon, white = hydrogen).

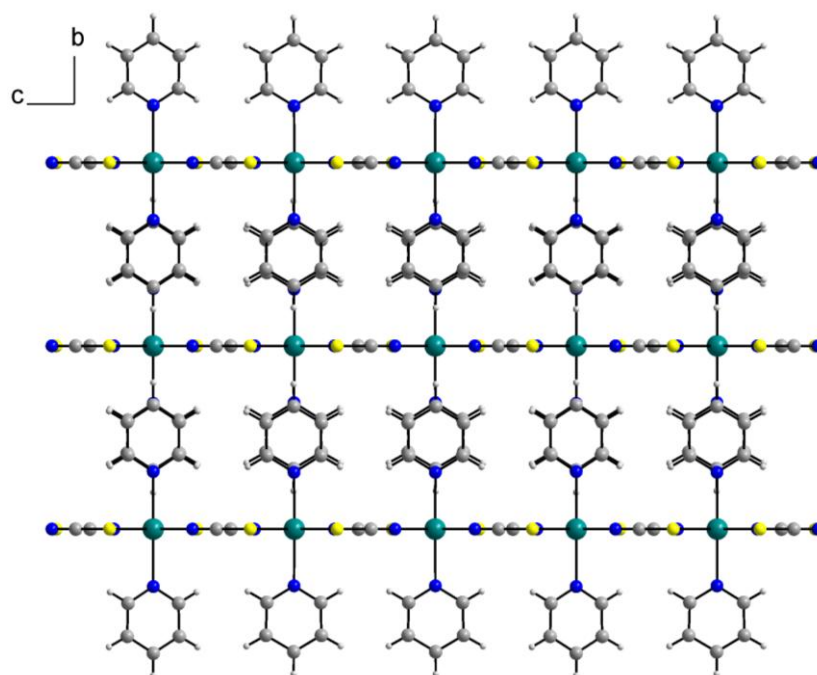


Figure S5. Crystal structure of **2-Cd/IV** with view along the crystallographic *a*-axis (green = cadmium, blue = nitrogen, yellow = sulfur, grey = carbon, white = hydrogen).

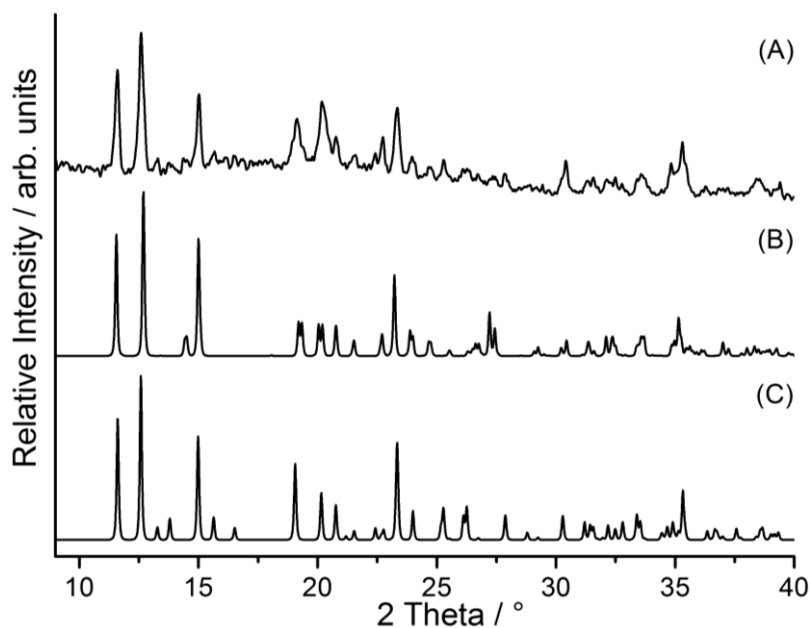


Figure S6. Experimental X-ray powder pattern (XRPD) of a mixture of single crystals of **2-Cd/II** and **2-Cd/IV** (A) and X-ray powder pattern of **2-Cd/II** (B) as well as **2-Cd/IV** (C) calculated from single-crystal data.

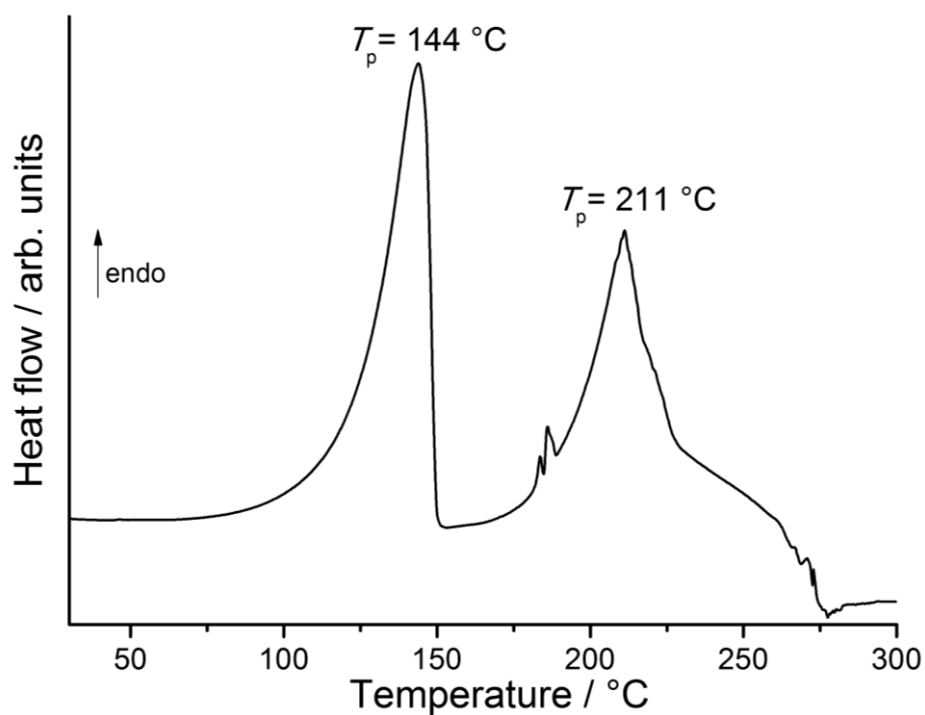


Figure S7. DSC curve for [Cd(NCS)₂(pyridine)₄] (**1-Cd**).

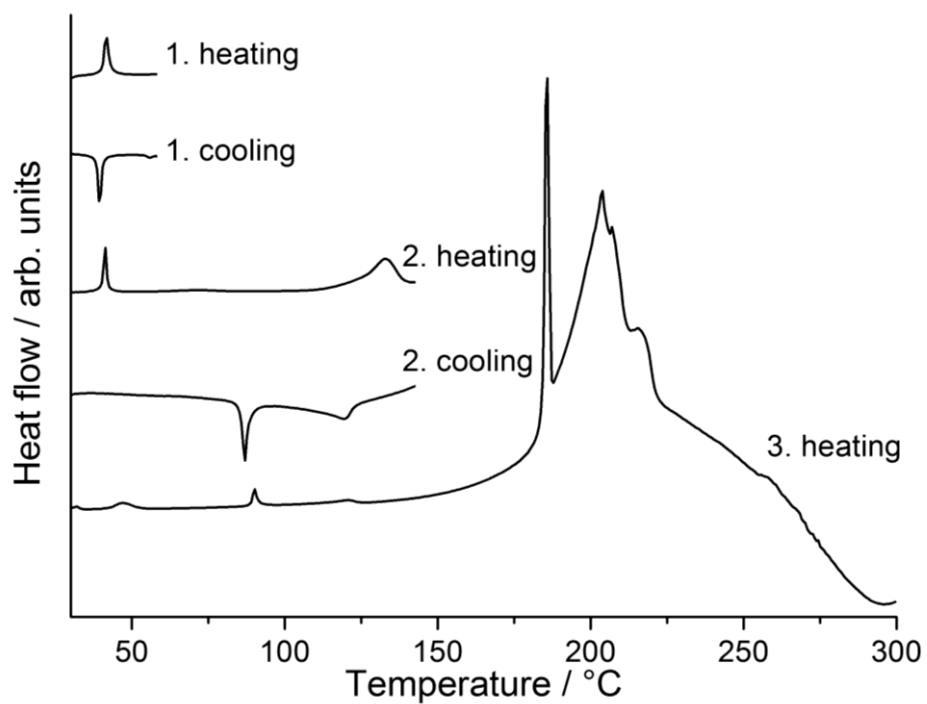


Figure S8. DSC heating and cooling cycles for [Cd(NCS)₂(pyridine)₂]_n (**2-Cd/II**).

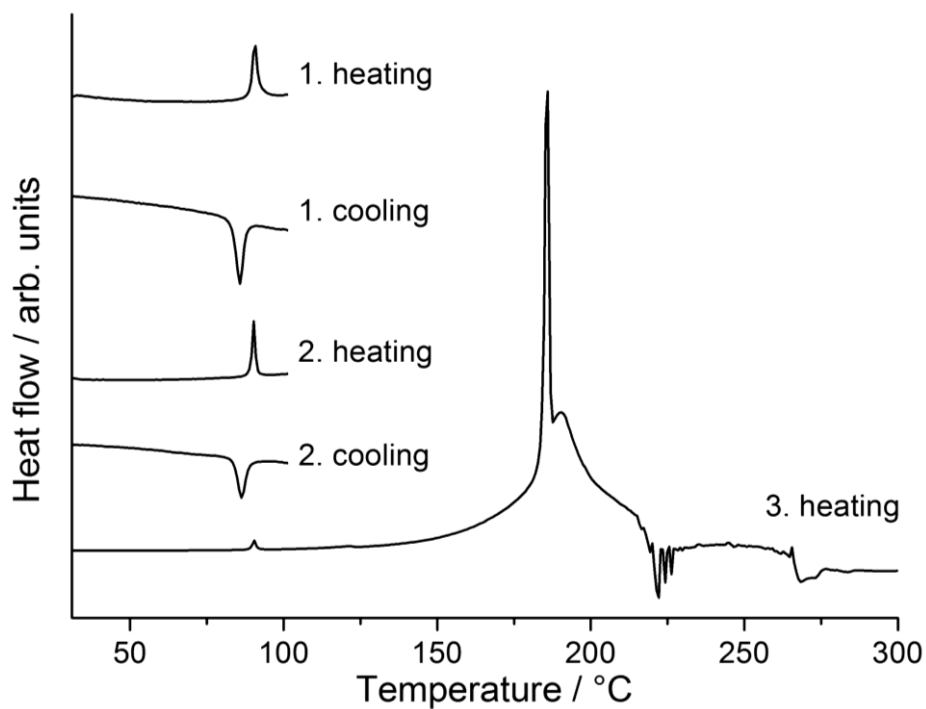


Figure S9. DSC heating and cooling cycles for [Cd(NCS)₂(pyridine)₂]_n (**2-Cd/III**).

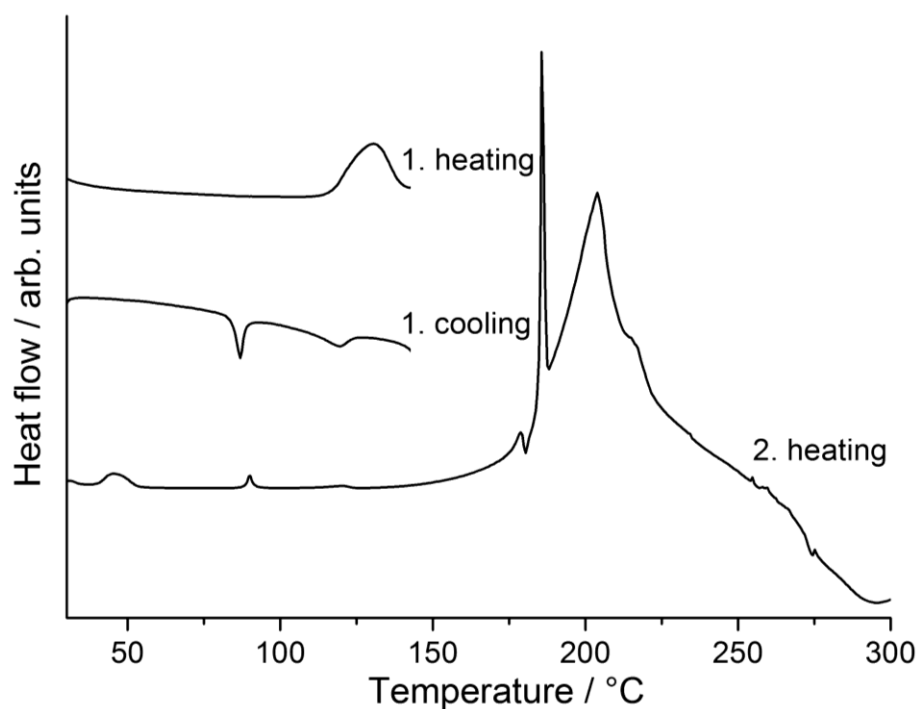


Figure S10. DSC heating and cooling cycles for $[\text{Cd}(\text{NCS})_2(\text{pyridine})_2]_n$ (**2-Cd/IV**).

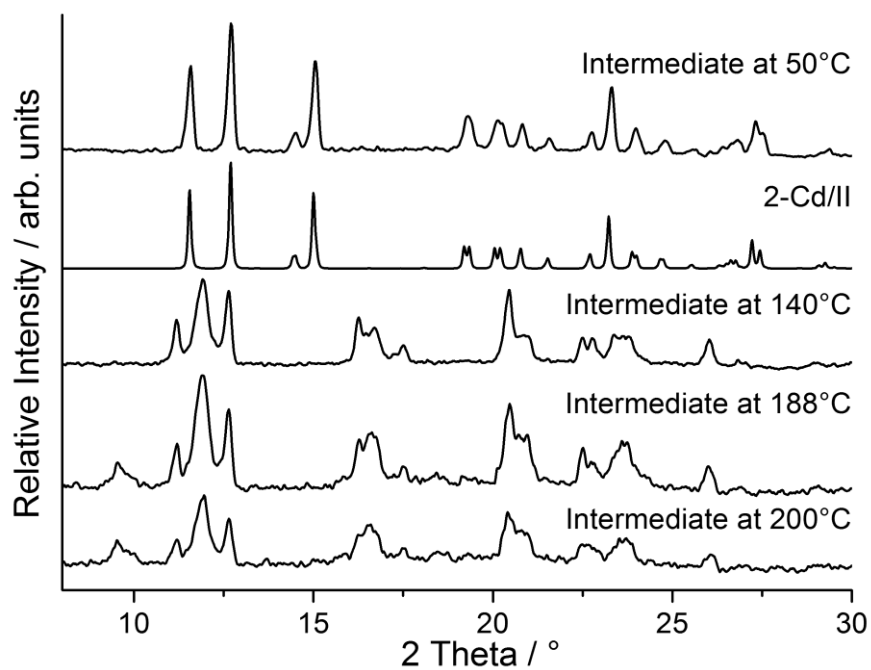


Figure S11. X-ray powder pattern of the intermediates obtained at different temperatures in the DSC measurement of compound **2-Cd/II** and X-ray powder pattern of $[\text{Cd}(\text{NCS})_2(\text{pyridine})_2]_n$ (**2-Cd/II**) calculated from single-crystal data.

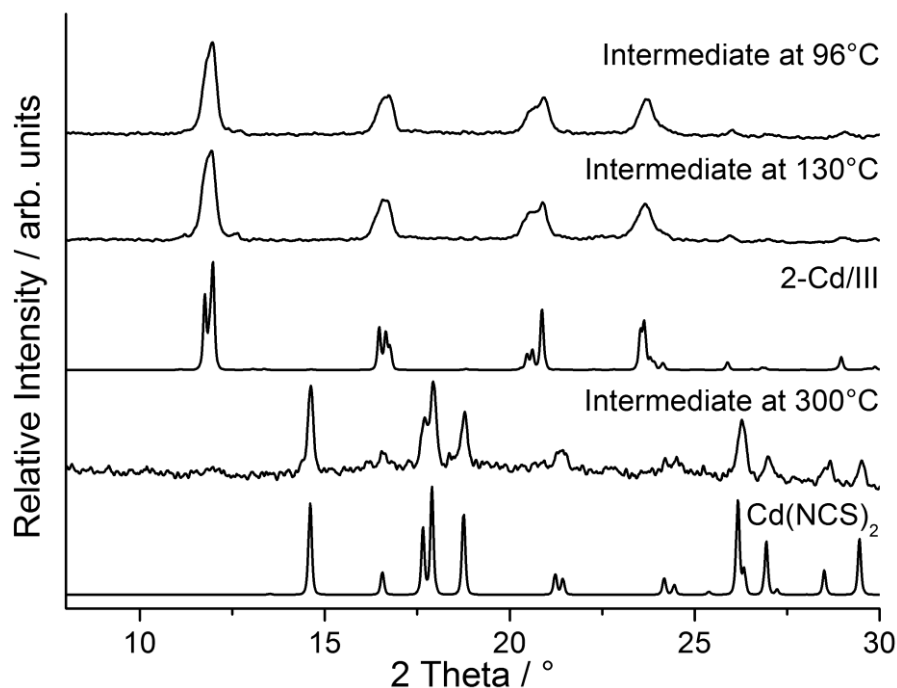


Figure S12. X-ray powder pattern of the intermediates obtained at different temperatures in the DSC measurements of compound **2-Cd/III** and X-ray powder pattern of $[\text{Cd}(\text{NCS})_2(\text{pyridine})_2]_n$ (**2-Cd/III**) calculated from Rietveld refinement and of $\text{Cd}(\text{NCS})_2$ calculated from single-crystal data.

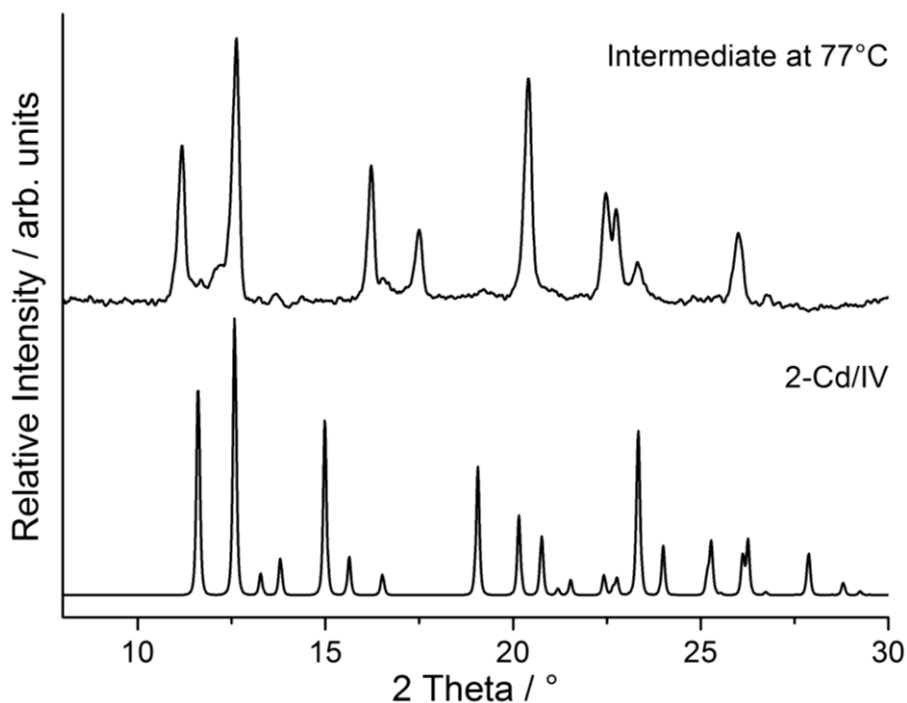


Figure S13. X-ray powder pattern of the intermediate obtained at 77°C from the DSC measurement of compound **2-Cd/IV** (top) as well as the X-ray powder pattern calculated for $[\text{Cd}(\text{NCS})_2(\text{pyridine})_2]_n$ (**2-Cd/IV**) from single-crystal data.

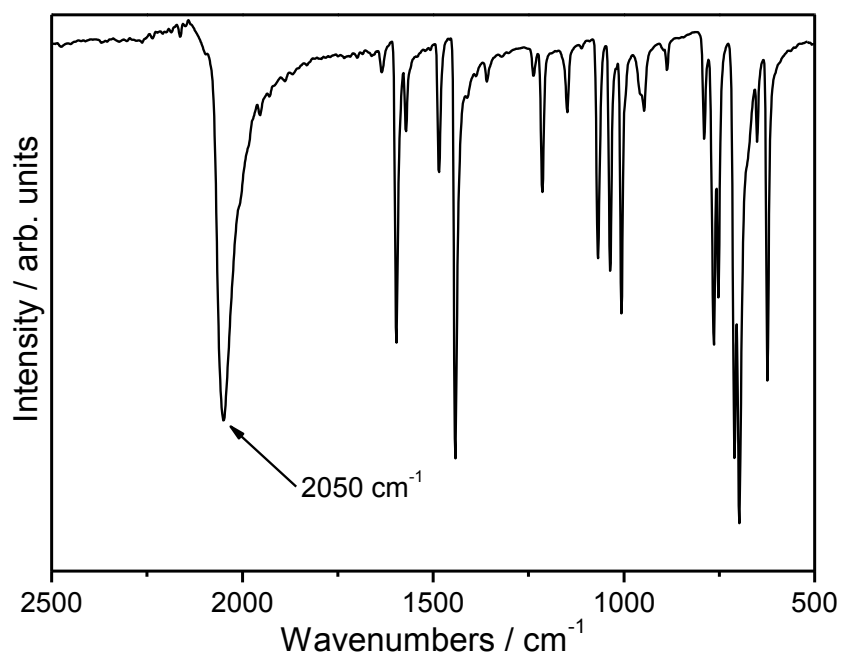


Figure S14. IR spectrum of [Cd(NCS)₂(pyridine)₄] (**1-Cd**).

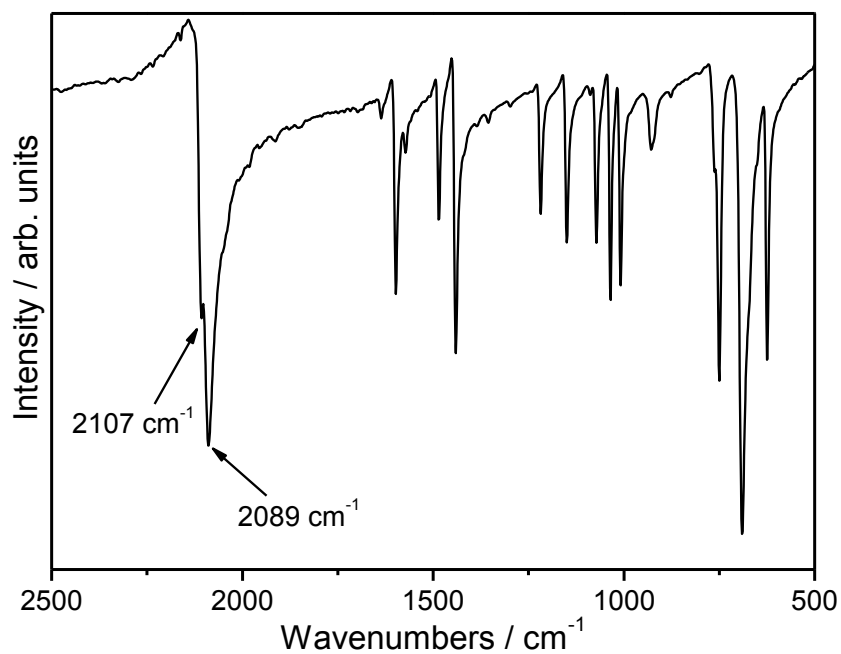


Figure S15. IR spectrum of the ligand-deficient 1:2 compound [Cd(NCS)₂(pyridine)₂]_n (**2-Cd/II**).

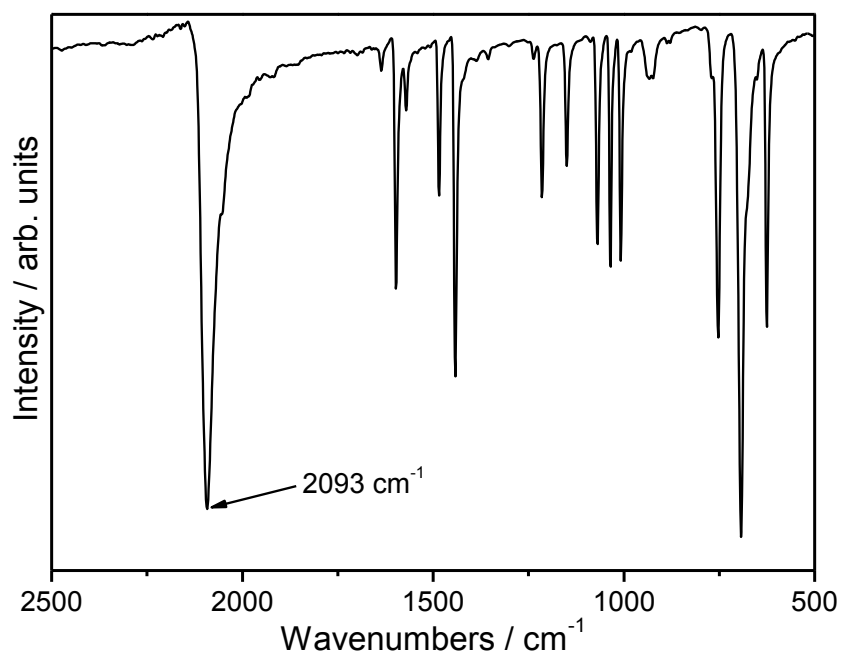


Figure S16. IR spectrum of $[\text{Cd}(\text{NCS})_2(\text{pyridine})_2]_n$ (**2-Cd/III**).

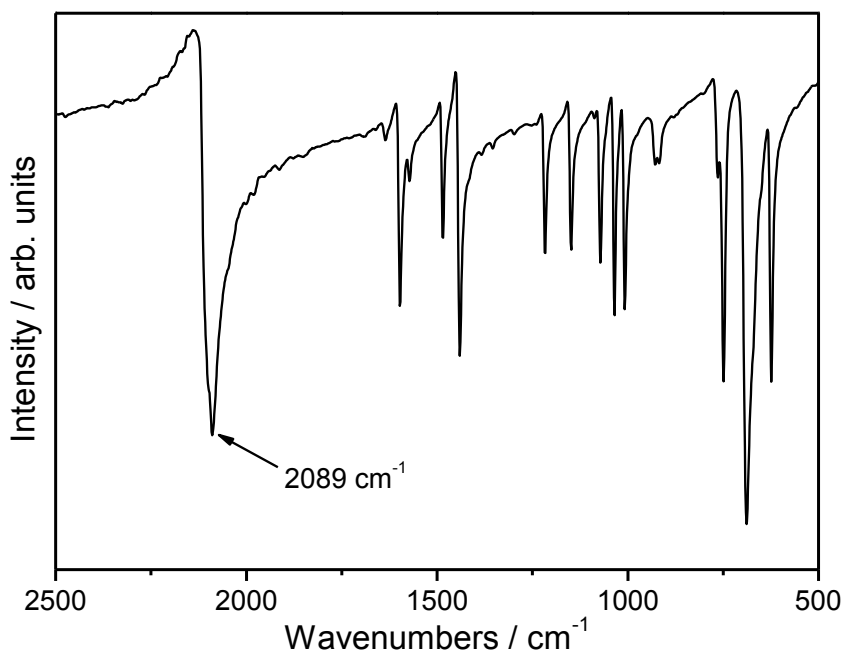


Figure S17. IR spectrum of $[\text{Cd}(\text{NCS})_2(\text{pyridine})_2]_n$ (**2-Cd/IV**).

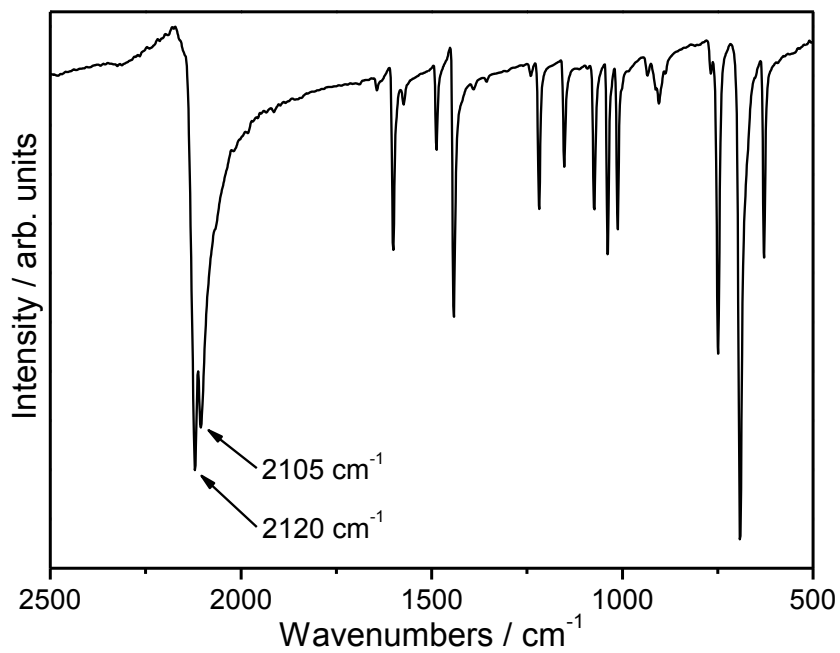


Figure S18. IR spectrum of $[\text{Cd}(\text{NCS})_2(\text{pyridine})]_n$ (**3-Cd**).